DNA Release Dynamics from Bioreducible Poly(amido amine) Polyplexes

Lei Wan,[‡] Yezi You,[§] Yi Zou,[‡] David Oupický,[§] and Guangzhao Mao*,[‡]

Department of Chemical Engineering and Materials Science, and Department of Pharmaceutical Sciences, Wayne State University, Detroit, Michigan 48202

Received: February 27, 2009; Revised Manuscript Received: May 8, 2009

The DNA release dynamics of bioreducible poly(amido amine) polyplexes were studied in real time by atomic force microscopy (AFM). DNA release is triggered by a depolymerization of high-molecular-weight polycations into low-molecular-weight oligocations that occurs by means of the thiol and disulfide exchange reaction mechanism. AFM images were captured in a simulated physiological reducing environment that used dithiothreitol. Distinctive stages of disassembly are common among various polyplexes that have different disulfide content, molecular weight, and polymer architecture, while the DNA release rate depends upon the disulfide content. In the first stage, polyplexes evolve from metastable structures into the more stable toroid structure upon the depolymerization. In the second stage, toroids either aggregate or fuse into larger toroids. In the last stage, DNA wormlike chains and loops are held by a central compact core. The results confirm the prospect of bioreducible poly(amido amine)s as controlled DNA delivery vectors. The study offers new physical insights into the DNA release pathway including intermediate structures that have a high degree of structural heterogeneity and disassembly induced particle growth. The study identifies disassembly induced colloidal and morphological instability as an important issue to be addressed.

Introduction

One area of research on polyelectrolyte complexes is layer-by-layer (LbL) assembly of bolaform amphiphiles and polyelectrolytes caused by electrostatic attraction of the hydrophilic headgroups and by short-range van der Waals attraction among the nonpolar chains.[1−4] That research has contributed to a promising method for localized gene delivery, that is, the incorporation of plasmid DNA polyanion into the LbL assembly.[5−7] An alternative method for gene delivery involves the DNA/polycation complexes. Mixing of DNA and a polycation in aqueous solution results in a homogeneous solution containing nanosized polyplexes. Our research is focused on the molecular disassembly process through which DNA is released from the LbL films and polyplexes. Molecular disassembly of polyplexes constitutes a critical step along a nonviral gene delivery pathway. In addition to the effect of polyplex particle size,[8,9] the timing and the degree of DNA release have been shown to affect transgene expression efficiency.[10−13]

In this study, the DNA release is triggered by a depolymerization of high-molecular-weight disulfide-containing polycations into low-molecular-weight α,ω-dithiol-oligocations that proceeds by the thiol and disulfide exchange reaction mechanism. Poly(amido amine)s with disulfide linkages were synthesized. Their polyplexes displayed low cytotoxicity and significantly higher transfection than those without a disulfide linkage.[14−16] The bioreducible polymers are less sensitive to hydrolysis than hydrolytically degradable polymers, such as poly(amino ester)s, and their polyplexes are expected to only release DNA rapidly inside the cell. The degradation of disulfide-containing polycations can be triggered by the redox potential gradient between extracellular environment and various subcellular organelles in states compatible with the physiological conditions.[17−22] Bioreducible poly(amido amine)s in the linear and hyperbranched forms have been synthesized by Michael addition copolymerization reaction.[23] With secondary and tertiary amines in the polymer backbone, poly(amido amine)s possess a high buffering capacity, which enables endosomal escape of the gene delivery vectors.[24] The LbL films of a hyperbranched poly(amido amine) and DNA showed higher and prolonged transfection than control polyethylenimine (PEI)-containing films in vitro and exhibited promising transfection activity in vivo.[6] Hyperbranched polymers can have higher molecular weights than similar linear polymers.[6,14,16,25] The higher molecular weight of hyperbranched polycations is expected to increase the stability and transfection activity of the DNA delivery vectors especially in vivo.

Recently, we used atomic force microscopy (AFM) to visualize plasmid DNA in various decondensed states from reducible polypeptide polyplexes under simulated physiological reducing conditions.[26] Prior to our work, AFM was mainly used to study DNA condensation and self-assembled nanostructure of polyplexes.[27−37] Our study revealed new molecular disassembly dynamics including the existence of intermediate structures with a high degree of structural heterogeneity, disassembly induced aggregation, and the dependence of the DNA release rate on polymer structure and solution conditions. Striking differences between polyplexes based on polypeptides of histidine-rich peptide HRP (CKHHHKHHHKC) and nuclear localization signal NLS (CGAGPKKKRKVC) peptide were captured by AFM, in real time and at the single polyplex level. The HRP and NLS polyplexes were similar in their initial morphology; a majority of them contained only one DNA plasmid. Upon reductive degradation by dithiothreitol (DTT), DNA was released from NLS abruptly regardless of the initial polyplex morphology, while DNA release from HRP polyplexes displayed a gradual decondensation that was dependent on the size of polyplexes. HRP polyplexes also displayed cooperative

* Corresponding author. E-mail: gzmao@eng.wayne.edu.
[‡] Department of Chemical Engineering and Materials Science.
[§] Department of Pharmaceutical Sciences.

10.1021/jp901835u CCC: $40.75
Published on Web 06/12/2009

SCHEME 1: Molecular Structures of Linear and Hyperbranched Poly(amido amine)s (Where the Disulfide Bond Content Is Varied by the Feed Molar Ratio of Non-reducible Monomer CBA (R1) to Non-reducible Monomer MBA (R2))

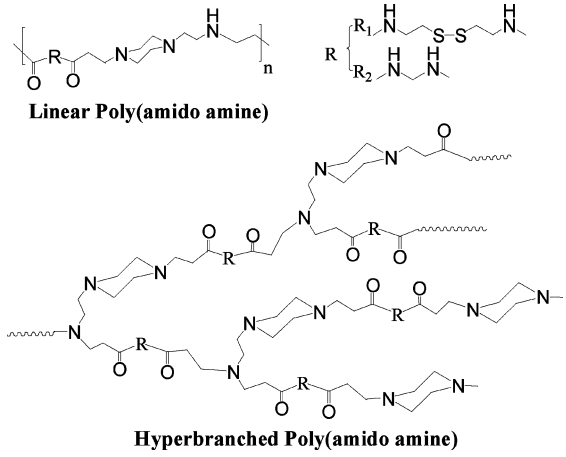

release behavior where smaller HRP polyplexes became unstable when they were in contact with neighboring decondensed chains.

This paper describes an AFM investigation of polyplexes undergoing reductive molecular disassembly that contain poly(amido amine)s in linear and hyperbranched forms. The chemical composition of the polymer is varied by the reducible monomer to nonreducible monomer ratio during synthesis. Distinctive stages of polyplex disassembly are revealed that are common among the polyplexes although the DNA release rate depends upon the disulfide content and perhaps also upon the polymer architecture. The results confirm the prospect of bioreducible poly(amido amine)s as controlled DNA delivery vectors and offer new insights into DNA release dynamics relevant to in vitro and in vivo gene delivery.

Experimental Methods

Materials. Plasmid DNA vector, gWiz high-expression luciferase, containing luciferase reporter gene, was purchased from Aldevron. The contour length of DNA with 6732 base pairs is estimated to be 2.3 μm. Dithiothreitol (DTT, Sigma), 1-(2-aminoethyl)piperazine (AEPZ, Aldrich), 1-methylpiperazine (Aldrich), *N,N′*-methylenebisacrylamide (MBA, Aldrich), and *N,N′*-cystaminebisacrylamide (CBA, Polysciences) were purchased in the highest commercially available purity and used without further purification. All other chemicals were purchased from Sigma-Aldrich. Water was deionized to 18 MΩ × cm resistivity using the Nanopure system from Barnstead. Grade V5 muscovite mica was purchased from Ted Pella and was hand cleaved just before use.

Synthesis of Bioreducible Hyperbranched and Linear Poly(amido amine)s. The synthesis of hyperbranched and linear bioreducible poly(amido amine)s by Michael addition copolymerization was reported in an earlier paper.[6] The different reactivity of the amines in AEPZ allows synthesis of either linear or hyperbranched polymers by simply changing the ratio of AEPZ-to-bisacrylamide monomers.[23] A 1:2 molar ratio of AEPZ to CBA + MBA yields hyperbranched polymers, while a 1:1 ratio leads to linear polymers (Scheme 1). The chemical composition of the hyperbranched polymers is further varied by the CBA to MBA ratio, that is, the reducible disulfide chain density. Table 1 lists the chemical composition and molecular weight characteristics of all of the poly(amido amine)s studied here. The chemical composition was characterized by ^{1}H NMR and ^{13}C NMR using a Varian spectrometer (400 MHz; see Supporting Information). Number-average (M_n) and weight-average (M_w) molecular weights and polydispersity index (M_w/M_n) were determined by size exclusion chromatography (SEC) in 0.03 M sodium acetate (pH 4.5) using Shimadzu LC-10ADVP liquid chromatography equipped with a CTO-10ASVP Shimadzu column oven and Polymer Laboratories PL gel 5 mm mixed C column. SEC data were analyzed using Astra 5.3.1.4 software from Wyatt Technology. Refractive index increments (d_n/d_c) were determined by an interferometric refractometer and used in SEC analysis.

TABLE 1: Chemical Composition and Molecular Weight Characteristics of Poly(amido amine)s

polymer	CBA content (% mol)	M_W	M_W/M_N
RHB1	0	50 000	3.8
RHB2	15	115 000	6.4
RHB3	21	32 000	2.2
RHB4	32	66 000	1.7
RHB5	48	40 000	3.3
RHB6	100	127 000	2.2
RL1	0	25 200	1.8
RL2	15	54 500	3.8
RL3	100	20 800	3.8

The low cytotoxicity of the bioreducible polymers is the primary motivation for this study. Cytotoxicity of the synthesized polycations and control PEI were estimated by measuring cell viability at 50 μg/mL of the polymer. All of the bioreducible poly(amido amine)s had lower cytotoxicity than control branched polyethylenimine (PEI, 25 kDa), and their cytotoxicity decreased with increasing content of the reducible disulfide bonds (data not shown).

Polyplex Preparation. The structure of polyplexes is sensitive to preparation conditions.[38,39] Here, 20 mg/L DNA solution in 0.03 M sodium acetate buffer (pH 4.5) was used to prepare polyplexes at the desired amine-to-DNA phosphate molar ratio (N/P). The poly(amido amine) was added to the DNA solution and mixed by vortexing at 3200 rpm (Fisher Scientific Vortex Mixer) for 10 s, and the solution was incubated at room temperature for 30 min.

AFM Characterization. AFM imaging was conducted using a Nanoscope III MultiMode atomic force microscope from Digital Instruments. Tapping Mode was performed in liquid using silicon nitride probes (NP, VEECO) with a nominal radius of curvature of 20 nm and cantilever spring constant of 0.38 N/m as provided by the manufacturer. A 20 μL sample of polyplex solution was placed on approximately 1 cm^2 of freshly cleaved mica. Excess solution was removed after 2 min, and the surface was rinsed with deionized water. The adsorbed polyplexes were always imaged in the same buffer (0.03 M sodium acetate) and at the same ionic strength as the reducing solution prior to reduction in order to be certain of the polyplex stability and to minimize any tip disturbance. Usually, the polyplexes were imaged in 40 μL of buffer solutions before 10 μL of DTT solution was injected. The final DTT concentration was maintained at 0.02 M in the liquid cell, which is at a similar level as the in vivo glutathione concentration in the nucleus.[40] AFM imaging ensued immediately after the introduction of DTT. The surface was imaged continuously at an average rate of 1.5−2 Hz on a 2 × 2 μm^2 until no significant changes occurred at the surface. The commonly used frequency, amplitude, integral, and proportional gains are approximately 8 kHz, 0.5−1 V, 0.5−2, and 0.75−3, respectively.

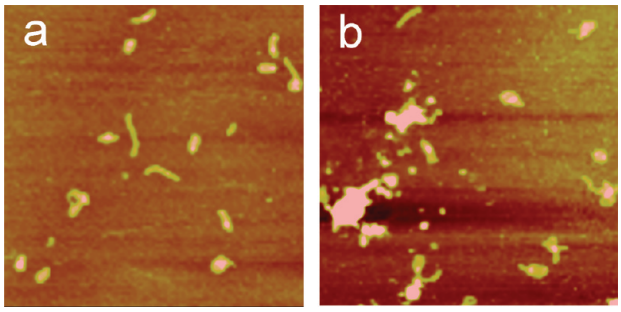

Figure 1. AFM height images of RL2/DNA polyplexes (N/P = 4) formed at incubation times of (a) 10 min and (b) 60 min. The images were captured in Tapping Mode in air. The scan size is 2 μm, and the z range is 10 nm.

The AFM images were analyzed using Nanoscope software version 5.12b by Veeco. The bearing analysis command in Nanoscope software was used to measure the particle volume and area in which the substrate was used as the threshold bearing plane. The particle volume above the threshold plane was calculated by integrating the depth histogram over the entire area above the threshold plane. The dynamic particle size results have a typical error of 30%. The apparent particle volume in our AFM analysis is higher than the actual volume because of the well-known tip-convolution effect. Alternatively, the particle volume can be determined by considering only the top half of the structure.[48] In the case of cap-shaped objects likely adopted by the polyplexes after adsorption, this method could lead to an underestimation of the particle size.

Results

Effect of Incubation Time. An incubation time of 30 min yielded the largest population of compact and nonaggregated polyplex structure. Accordingly, an incubation time of 30 min was chosen for the preparation of all polyplexes. A shorter incubation time yielded a significant amount of uncondensed and rod structure while significant aggregation occurred at longer than 30 min incubation time (Figure 1). Others have also reported a larger percentage of rods near the start of incubation due to the more favorable formation kinetics of rods.[41]

Morphology of As-formed Polyplexes. The morphology and size distribution of as-formed polyplexes adsorbed on mica were studied by AFM tapping mode in deionized water. All bioreducible poly(amido amine)s were capable of condensing plasmid DNA into nanosized polyplexes at N/P > 2 and an incubation time of 30 min. No significant morphological differences were observed among polyplexes formed with the various poly(amido amine)s. The common morphology and size features are described here. Our results are similar to those reported previously using different multivalent condensing agents.[30,34,37,42]

Figure 2 presents representative polyplex shapes and sizes together with their bearing volume histogram. The toroid structure is characterized by a distinctive hole in the middle. The spheroid is a globular structure without that central hole. The rod is an elongated object whose diameter and length are similar to the diameter and circumference of the toroid. The largest population of the polyplexes has a size range of $1-2 \times 10^4$ nm^3. This range matches the theoretical volume of a closely packed polyplex containing a single plasmid DNA with 6732 bp, 1.4×10^4 nm^3. The theoretical value was calculated by assuming an interhexagonal separation between neighboring polycation and DNA chain of 2.7 nm.[43] Thus, we can conclude that the largest population, regardless of morphology (toroid in Figure 2a, rod in Figure 2b, spheroid in Figure 2c), contains a single plasmid DNA; that is, it belongs to the monomolecular condensate. The particles with a volume range of $2-5 \times 10^4$ nm^3 contain 2−3 DNA plasmids and are also capable of forming toroids (represented by Figure 2d), rods, or folded toroids (represented by Figure 2e), and spheroids (represented by Figure 2f). A small fraction of polyplexes contains more than 3 DNA molecules (represented by Figure 2g−i). The shape of these larger particles is ill defined. The larger particles are generally caused by partial condensation or polyplex aggregation.

DNA Release Dynamics. Next, we studied DNA release from polyplexes in real time by contacting the adsorbed polyplexes with the reducing DTT solution. The images were captured every 2 min from the time of DTT addition.

Both polyplexes and excess poly(amido amine)s are capable of adsorption on mica. But, the adsorption of the flexible poly(amido amine) results in a flat, featureless film. In the in situ AFM images, only the disassembly behavior of the polyplexes was resolved. The degradation of the poly(amido amine) was not. Prior to the injection of the DTT solution, the stability of the polyplexes was studied in aqueous buffer solutions containing up to 1 M NaCl. The structure of the polyplexes was unchanged for at least 1 h under repeated AFM scanning. It was concluded that salt alone was not able to induce decondensation.

Dynamic AFM experiments were carried out on all of the poly(amido amine) polyplexes, and the average DNA release times are listed in Table 2. The DNA release time was recorded as the time from DTT injection to the time when remaining features exhibited a height less than 3 nm, which corresponds to decondensed DNA chains adsorbed on substrate, or when the chain features disappeared from the image, which corresponds to complete desorption of DNA chains from the substrate. Only poly(amido amine)s containing the reducible disulfide bond were capable of releasing DNA, while the polyplexes formed with nonreducible poly(amido amines), that is, RL1 and RHB1, were stable in the DTT solution. The DNA release rate from polyplexes can be tuned from almost instant release to sustained release by varying the CBA content. Complete DNA release from RHB6 and RL3 polyplexes took only a few minutes while 170 min elapsed before DNA was completely released from RHB2 polyplexes. The slow release kinetics of RHB2 polyplexes made it more feasible to study the intricate and multistep DNA release dynamics. By assuming that the disulfide reaction with DTT is not the rate limiting step, the release rate is a function of oligocation chain length because the higher the CBA content the shorter the average chain length after the reduction reaction. DNA release from RHB2 polyplexes is slower than that from RL2 counterparts even though they have similar disulfide contents. There is insufficient evidence, however, to determine whether the difference is due to polymer architecture, that is, hyperbranched versus linear, or molecular weight difference.

Now we discuss the details of morphological changes during polyplex disassembly. Upon DTT introduction, polyplexes of various shapes tended to converge into the toroid form during the first 10 min prior to visible DNA release. Figure 3 shows such a transition of a rodlike object to toroid. It gradually opens up in the center. The rod has a smaller length to width aspect ratio, 2.6, than that of a typical rod however. Figure 4 shows a similar transition to the toroid form by a spheroid with a small arm. With time, the spheroid gradually developed a central hole and incorporated the outstretched arm into the single toroid. In contrast, the toroid on the left remained unchanged. Figure 5

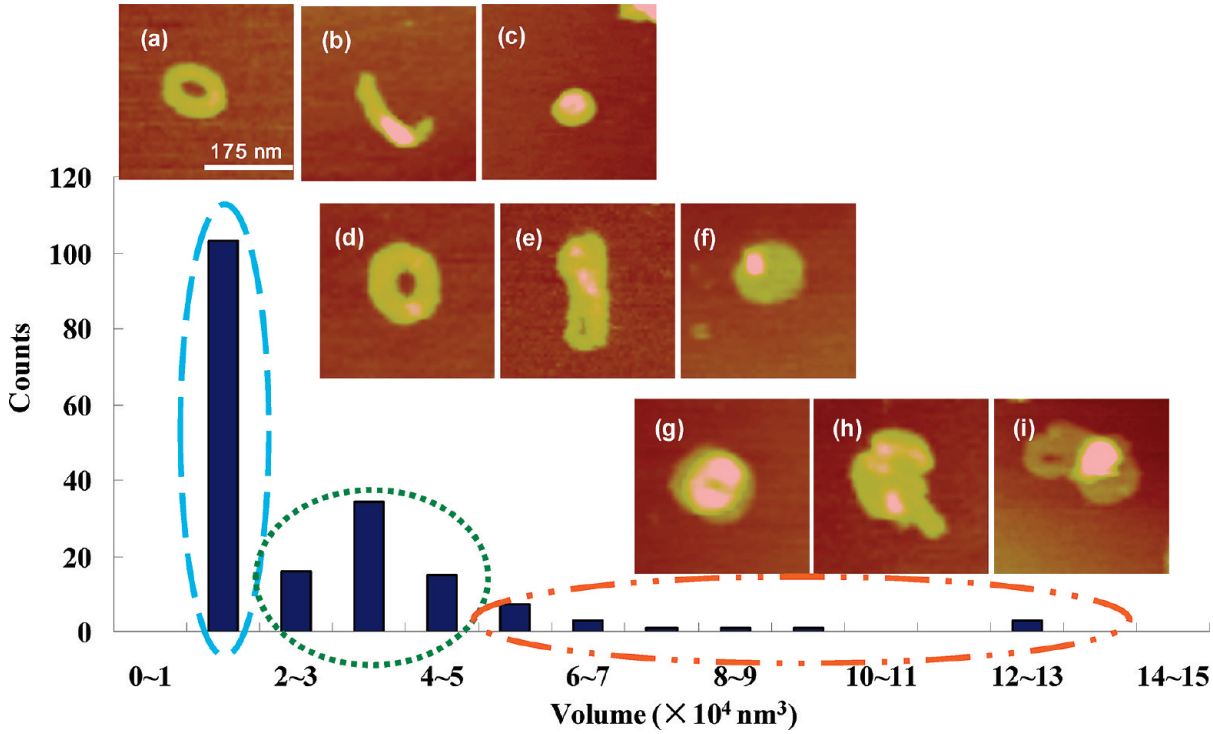

Figure 2. AFM bearing volume histogram and representative AFM height images of the bioreducible polyplexes (N/P = 4). The images were captured in Tapping Mode in deionized water. The bearing size of polyplexes in solution has a typical error of 30%. The scan size is 350 nm. The z range is 15 nm for (g) to (i) and is 8 nm for all others. Polyplexes whose volume is in the range of $1-2 \times 10^4$ nm^3 are represented by (a−c). Polyplexes whose volume is in the range of $2-5 \times 10^4$ nm^3 are represented by (d−f). Polyplexes whose particle volume is greater than 5×10^4 nm^3 are represented by (g−i). (a), (e), and (i) are RHB3/DNA polyplexes, and all others are RHB2/DNA polyplexes.

TABLE 2: DNA Release Rate Dependence on Chemical Composition and Polymer Chain Architecture[a]

CBA content (%)	100	48	32	21	15	0
hyperbranched poly(amido amine)	<2 min	~5 min	~30 min	~50 min	~170 min	no disassembly
linear poly(amido amine)	<2 min				~50 min	no disassembly

[a] The reducing solutions consists of 0.02 M DTT, 0.2 M NaCl, and 0.03 M sodium acetate buffer (pH = 4.5).

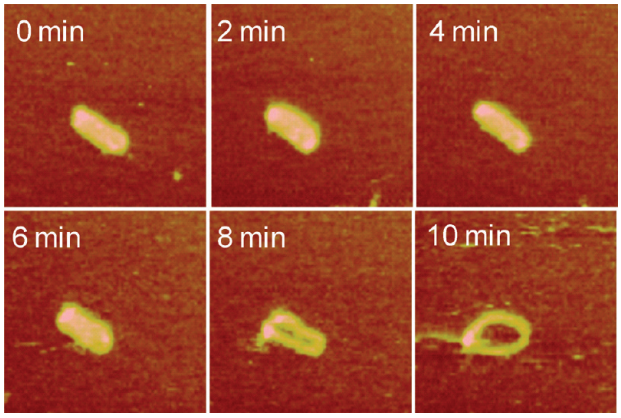

Figure 3. Real-time AFM images showing a gradual transition of a single rodlike RHB3/DNA polyplex to a toroid with a well-defined central hole captured in the DTT solution. Time zero corresponds to the injection of the DTT solution. The scan size is 500 nm. The z range is 7 nm.

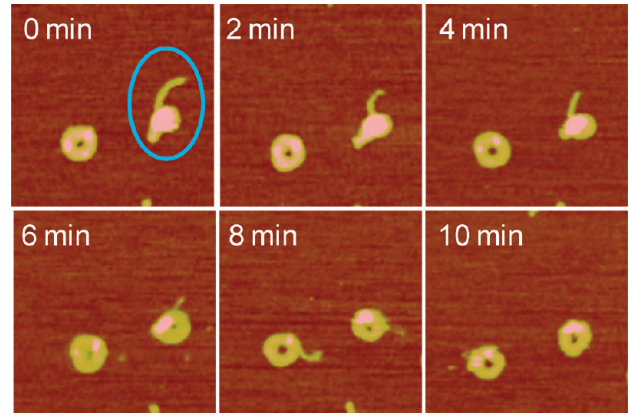

Figure 4. Real-time AFM images showing a gradual transition of a single spheroid RHB4/DNA polyplex (circled) to a toroid captured in the DTT solution. The scan size is 600 nm. The z range is 8 nm.

presents images of multiple polyplexes undergoing morphological transitions upon the addition of the DTT solution. The transition from compact structure to toroid with increasing diameter is evident (see particles marked by A). Larger particles containing more than one DNA plasmid also display the same trend toward the formation of toroid, for example, particle marked by B. Particle B ultimately disentangled into several toroids (t = 70 min). The polyplexes also display mutual interactions during disassembly. The object marked by C was composed of aggregated spheroid−toroid−rod. It first developed into three distinct toroids (t = 36 min), and then the three toroids fused into one larger object (t = 53 min). Initially separated polyplexes, marked by D, were capable of forming connections with each other and eventually merged into each other during disassembly.

Figure 6 provides another example of disassembly induced particle−particle interaction and aggregation. The two attached

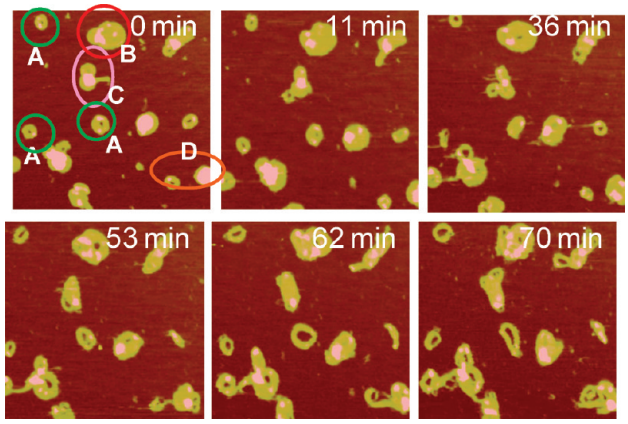

Figure 5. Real-time AFM images of RHB2/DNA polyplexes captured after the introduction of the DTT solution. Images were continuously captured every 2−5 min but only selective images are shown. The scan size is 1.5 μm. The z range is 10 nm.

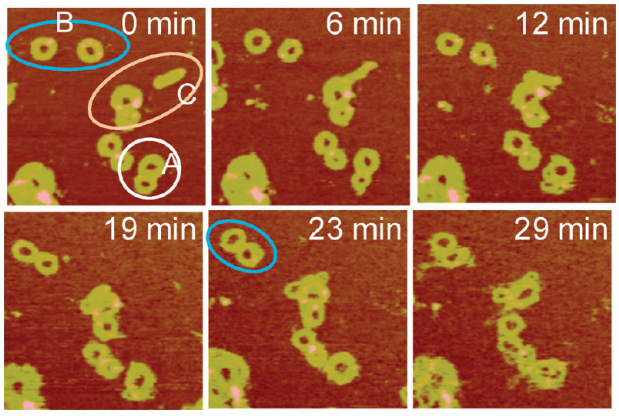

Figure 6. Real-time AFM images of RL2/DNA polyplexes in the DTT solution showing particle−particle interaction and aggregation. Images were continuously captured every 2−5 min but only selective images are shown. The scan size is 1 μm, and the z range is 10 nm.

toroids prior to the addition of DTT (marked by A) merged into one 12 min later, and the merged toroid attached to another group 23 min later. The initially far apart toroids, separated by ~100 nm from each other (marked by B), were capable of attaching to each other during the observation period. The group of polyplexes (marked by C) demonstrates both mutual attraction and fusion. The rod polyplex first attached to the neighboring toroid (t = 6 min), and reoriented to the tangential direction of the toroid host (t = 12 min) before fusing into the host (t = 19 min). During particle fusion, there is little loss in the overall particle volume. The overall volume changed from 4.8×10^4 nm^3 to 4.4×10^4 nm^3 and from 9.0×10^4 nm^3 to 8.6×10^4 nm^3 for group A and C respectively.

Following morphological changes and fusion as described above, the bioreducible polyplexes underwent the final DNA decondensation and release transition. DNA decondensation is signified by thin wormlike chains emerging from the polyplexes. Figure 7 presents a typical DNA release sequence from the RHB2/DNA (N/P = 4) polyplex in the DTT solution. A significant number of DNA chains were released from the polyplexes at 68 min. The decondensed DNA chains are thinner than the condensed portion of the polyplex. Loose DNA chains continued to emerge and expand up to the end of the observation period. The various shapes of condensed polyplexes tend to evolve into a common decondensed structure containing a central core surrounded by loose DNA loops and chains. This common structure during polyplex disassembly resembles

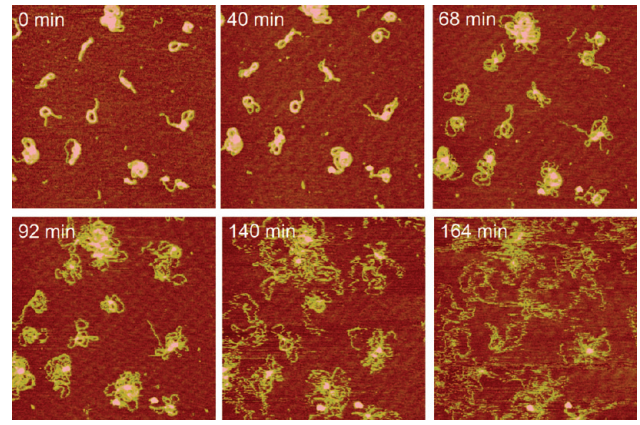

Figure 7. Real-time AFM images of RHB2/DNA polyplexes in the DTT solution showing the DNA decondensation stage. Images were continuously captured every 2−5 min but only selective images are shown. The scan size is 2 μm, and the z range is 6 nm.

closely the partially condensed DNA during polyplex assembly reported in literature. For example, Dunlap et al.[29] reported several partially condensed DNA structures including folded loops of DNA surrounding central cores, loose coils with isolated nodes, and bundles. The less condensed site was believed to be the initiation sites for enzymatic attack.[35]

Discussion

DNA condensation remains an active topic for experimental and theoretical research[44−49] because of its importance in cell biology, virology, polymer physics, and biotechnology. DNA condensation is driven by an entropy increase associated with the release of counterions upon the polyplex formation. The final condensate structure is determined by a variety of intermolecular forces including forces resisting condensation, such as bending, entropy loss upon demixing of polymer and solvent, and electrostatic repulsion among DNA chains, and favorable forces, such as correlated multivalent counterion fluctuation and cooperative hydration.[48] Manning's counterion condensation theory predicts that 90% of the DNA charges must be neutralized for condensation to occur.[50] In the reverse process of decondensation, when a sufficient number of binding cations are lost, DNA is released from the polyplex. Our experimental results confirm that the binding affinity dependence on polycation chain length is the main principle behind controlled DNA release by bioreducible polycations. However, the decondensation process does not appear to be instant as predicted for stiff polymers such as DNA, and the system exhibits a great deal of structural heterogeneity.

Various morphologies of DNA condensates have been reported including toroids, rods, spheroids, and less defined ones including rings and flower-like particles depending on condensing conditions, properties of DNA molecules, and condensing agents.[51] The polyplex formation is described by the nucleation and growth process.[45,52,53] It starts with the formation of a nucleation loop or rod followed by the intramolecular collapse of the entire DNA molecule to form a monomolecular toroid or rod. Monomolecular polyplexes grow into multimolecular toroids or rods by incorporating free DNA molecules.[53] Molecular simulations of DNA condensation show that the monomolecular toroid is more stable than the rod morphology.[54−56] Nucleation kinetics favor the rod form,[32,41] which is the reason why more rods were found at incubation times shorter than 30 min. Spheroids and flower-like polyplexes are often associated with high-molecular-weight polyelectrolytes[57,58] and are also

considered to be kinetically trapped. Polyplexes are unstable relative to the aggregated phase and they are expected to grow with time because of kinetic and thermodynamic factors.[41,42,59] In low salt conditions, polyplex formation is dominated by kinetics and its structure is trapped in far from its equilibrium state. The morphological instability of polyplexes represents one of the major obstacles for successful nonviral gene delivery systems.[13,60,61] Higher level aggregation can be a disadvantage for gene delivery because of the difficulty in trafficking large particles and the introduction of too many DNA fragments into one cell.

In our study, we found that the initial polyplex size and morphological distributions are rather insensitive to the polymer structure. For example, we observed toroids with average outer diameter of 100 nm in a wide range of molecular weights (25 000−130 000 g/mol) and disulfide content (0−100% CBA), as well as different chain architecture (linear vs hyperbranched). Our experimental evidence indicates that the polyplex formation is dominated by kinetic factors. The relative stability among the different forms also indicates that the activation energy from one to another is prohibitively high. The polyplexes were formed in dilute solution during vigorous mixing, which ensured small polyplex size. In addition, N/P ratios greater than 2 plus the highly charged nature of the poly(amindo amine)s resulted in overall positive zeta potential values (data not shown). The positive surface charge further limits particle growth during polyplex formation.

DNA release from the bioreducible polyplexes is triggered by a depolymerization process that converts high-molecular-weight poly(amido amine)s into low-molecular-weight oligomers and monomers. The polyplex becomes unstable; that is, the polyanion and polycation dissolve in solution, when the molecular weight of the polycation is greatly reduced. This chain length dependence originates from a loss of entropy as a result of a higher number of shorter chains bound to DNA. The depolymerization rate is much faster than the AFM time period.[62,63] Therefore, we interpret the polyplex morphologies after DTT injection as those exhibited by polyplexes containing low-molecule-weight cations. The experimental evidence points to the role of depolymerization in driving the transition from frozen states to the lowest energy state. When the high-molecular-weight polycation is converted to low-molecular-weight cations, the transition energy is lowered to allow different forms to converge into the lowest energy form, that is, the toroid structure. Depolymerization weakens the electrostatic interaction and enables rearrangement by freeing counterion from kinetically constrained binding sites. The chain length reduction results in a loss of excess cations thus allowing closer packing as well as the loss of the shell of the excess polycation that provides colloidal stabilization. The role of depolymerization in a sense is similar to that of salt. Our study shows that the toroid is the more stable form in the case of low-molecular-weight counterions for both monomolecular and multimolecular polyplexes. Since all of the in situ AFM experiments were conducted in DNA-free solutions, the structural transitions are accomplished without the free DNA, thus providing a new mechanism for DNA morphological transition and an alternative to the DNA-assisted mechanism.[41]

Polyplex interaction during disassembly is also interesting. Two neighboring polyplexes are attracted to each other and fuse into one. The interparticle interaction is facilitated by a reduction in the positive charges or a local charge reversal due to depolymerization. The same local charge reversal mechanism results in intersegment attraction in polyplex formation.[62,64] The less compact condensate starts to recover phosphate groups that make part of the chain negatively charged. The negatively charged DNA interacts electrostatically with positively charged condensate surface. The hydrophobic interaction may also play a role if oligocations rearrange to expose the hydrophobic parts as in the ladder structure initially proposed by Kabanov. The interparticle interaction and particle growth in our case are not mediated by free DNA. Instead, the same correlated electrostatic fluctuation and hydrophobic interactions between neighboring particles and chains are responsible. A previous study observed the commensurate reorganization of two DNA strands, which was considered as a precursor to the formation of a larger condensate.[31] The commensurate association may also play a role in DNA release dynamics, for example, the rod orientation from the radial to the tangential direction with respect to the nearby toroid before fusion (Figure 5 group C).

Conclusions

The bioreducible poly(amido amine) polyplexes provide an ideal system to study molecular disassembly and DNA decondensation dynamics by real-time AFM. The polyplexes are stable in the oxidizing environment representative of the nonreducing extracellular space. DNA release is triggered by mild DTT and salt concentrations compatible with the physiological environment. The results demonstrate DNA release dynamics from bioreducible polyplexes to consist of three stages that take place at different times. In the first stage, upon depolymerization, polyplexes evolve from metastable structures into the more favorable toroid structure. In the second stage, toroids interact with each other by aggregation and fusion. In the last stage, DNA gradually unravels from the polyplex resulting in highly decondensed wormlike chains and loops that are held by a central compact core. Our data demonstrate that the DNA release rate can be precisely controlled by the disulfide bond content. The effect of polymer architecture and molecular weight needs further investigation. The polyplex colloidal stability, the intermediate structure, and their interactions impact its delivery efficiency and its effect on cell viability. In order to mimic conditions in cytosol, future experiments will be conducted in conditions more closely resembling cytosol, for example, in glutathione instead of DTT.

Acknowledgment. This work was supported partially by National Science Foundation Grant CBET-0553533 and Grant CBET-0755654 (G.M.) and National Institutes of Health Grant CA 109711 from the National Cancer Institute (D.O.). The manuscript is dedicated to Professor H. Ted Davis on his 70th birthday.

Supporting Information Available: The typical ^{1}H NMR and ^{13}C NMR spectra of reducible hyperbranched poly(amido amine)s. This material is available free of charge via the Internet at http://pubs.acs.org.

References and Notes

(1) Decher, G.; Hong, J. D. *Berichte Der Bunsen-Gesellschaft-Physical Chemistry Chemical Physics* **1991**, *95*, 1430–1434.

(2) Mao, G. Z.; Tsao, Y. H.; Tirrell, M.; Davis, H. T.; Hessel, V.; Ringsdorf, H. *Langmuir* **1993**, *9*, 3461–3470.

(3) Mao, G. Z.; Tsao, Y. H.; Tirrell, M.; Davis, H. T.; Hessel, V.; Ringsdorf, H. *Langmuir* **1995**, *11*, 942–952.

(4) Mao, G. Z.; Tsao, Y. H.; Tirrell, M.; Davis, H. T.; Hessel, V.; Vanesch, J.; Ringsdorf, H. *Langmuir* **1994**, *10*, 4174–4184.

(5) Blacklock, J.; Handa, H.; Manickam, D. S.; Mao, G. Z.; Mukhopadhyay, A.; Oupicky, D. *Biomaterials* **2007**, *28*, 117–124.

(6) Blacklock, J.; You, Y.-Z.; Zhou, Q.-H.; Mao, G.; Oupicky, D. *Biomaterials* **2009**, *30*, 939–950.
(7) Kakade, S.; Manickam, D. S.; Handa, H.; Mao, G.; Oupicky, D. *Int. J. Pharm.* **2009**, *365*, 44–52.
(8) Petersen, H.; Kunath, K.; Martin, A. L.; Stolnik, S.; Roberts, C. J.; Davies, M. C.; Kissel, T. *Biomacromolecules* **2002**, *3*, 926–936.
(9) Vijayanathan, V.; Thomas, T.; Shirahata, A.; Thomas, T. J. *Biochemistry* **2001**, *40*, p 13644–13651.
(10) Schaffer, D. V.; Fidelman, N. A.; Dan, N.; Lauffenburger, D. A. *Biotechnol. Bioeng.* **2000**, *67*, 598–606.
(11) Kircheis, R.; Wightman, L.; Wagner, E. *Adv. Drug Delivery Rev.* **2001**, *53*, 341–358.
(12) Bettinger, T.; Carlisle, R. C.; Read, M. L.; Ogris, M.; Seymour, L. W. *Nucleic Acids Res.* **2001**, *29*, 3882–3891.
(13) Wiethoff, C. M.; Middaugh, C. R. *J. Pharm. Sci.* **2003**, *92*, 203–217.
(14) Lin, C.; Zhong, Z.; Lok, M. C.; Jiang, X.; Hennink, W. E.; Feijen, J.; Engbersen, J. F. J. *J. Controlled Release* **2006**, *116*, 130–137.
(15) Hoon Jeong, J.; Christensen, L. V.; Yockman, J. W.; Zhong, Z.; Engbersen, J. F. J.; Jong Kim, W.; Feijen, J.; Wan Kim, S. *Biomaterials* **2007**, *28*, 1912–1917.
(16) Christensen, L. V.; Chang, C. W.; Kim, W. J.; Kim, S. W.; Zhong, Z. Y.; Lin, C.; Engbersen, J. F. J.; Feijen, J. *Bioconjugate Chem.* **2006**, *17*, 1233–1240.
(17) Tang, F. X.; Hughes, J. A. *Bioconjugate Chem.* **1999**, *10*, 791–796.
(18) Byk, G.; Wetzer, B.; Frederic, M.; Dubertret, C.; Pitard, B.; Jaslin, G.; Scherman, D. *J. Med. Chem.* **2000**, *43*, 4377–4387.
(19) Saito, G.; Swanson, J. A.; Lee, K. D. *Adv. Drug Delivery Rev.* **2003**, *55*, 199–215.
(20) Read, M. L.; Bremner, K. H.; Oupicky, D.; Green, N. K.; Searle, P. F.; Seymour, L. W. *J. Gene Medicine* **2003**, *5*, 232–245.
(21) Chittimalla, C.; Zammut-Italiano, L.; Zuber, G.; Behr, J. P. *J. Am. Chem. Soc.* **2005**, *127*, 11436–11441.
(22) Oishi, M.; Hayama, T.; Akiyama, Y.; Takae, S.; Harada, A.; Yamasaki, Y.; Nagatsugi, F.; Sasaki, S.; Nagasaki, Y.; Kataoka, K. *Biomacromolecules* **2005**, *6*, 2449–2454.
(23) Wu, D. C.; Liu, Y.; Chen, L.; He, C. B.; Chung, T. S.; Goh, S. H. *Macromolecules* **2005**, *38*, 5519–5525.
(24) Boussif, O.; Lezoualch, F.; Zanta, M. A.; Mergny, M. D.; Scherman, D.; Demeneix, B.; Behr, J. P. *Proc. Natl. Acad. Sci. U.S.A.* **1995**, *92*, 7297–7301.
(25) Jeong, J. H.; Christensen, L. V.; Yockman, J. W.; Zhong, Z. Y.; Engbersen, J. F. J.; Kim, W. J.; Feijen, J.; Kim, S. W. *Biomaterials* **2007**, *28*, 1912–1917.
(26) Wan, L.; Manickam, D. S.; Oupicky; #x301, D.; Mao, G. *Langmuir* **2008**, *24*, 12474–12482.
(27) Wolfert, M. A.; Seymour, L. W. *Gene Ther.* **1996**, *3*, 269–273.
(28) Allen, M. J.; Bradbury, E. M.; Balhorn, R. *Nucleic Acids Res.* **1997**, *25*, 2221–2226.
(29) Dunlap, D. D.; Maggi, A.; Soria, M. R.; Monaco, L. *Nucleic Acids Res.* **1997**, *25*, 3095–3101.
(30) Hansma, H. G.; Golan, R.; Hsieh, W.; Lollo, C. P.; Mullen-Ley, P.; Kwoh, D. *Nucleic Acids Res.* **1998**, *26*, 2481–2487.
(31) Ono, M. Y.; Spain, E. M. *J. Am. Chem. Soc.* **1999**, *121*, 7330–7334.
(32) Martin, A. L.; Davies, M. C.; Rackstraw, B. J.; Roberts, C. J.; Stolnik, S.; Tendler, S. J. B.; Williams, P. M. *FEBS Lett.* **2000**, *480*, 106–112.
(33) Iwataki, T.; Kidoaki, S.; Sakaue, T.; Yoshikawa, K.; Abramchuk, S. S. *J. Chem. Phys.* **2004**, *120*, 4004–4011.
(34) Danielsen, S.; Maurstad, G.; Stokke, B. T. *Biopolymers* **2004**, *77*, 86–97.
(35) Chim, Y. T. A.; Lam, J. K. W.; Ma, Y.; Armes, S. P.; Lewis, A. L.; Roberts, C. J.; Stolnik, S.; Tendler, S. J. B.; Davies, M. C. *Langmuir* **2005**, *21*, 3591–3598.
(36) Maurstad, G.; Danielsen, S.; Stokke, B. T. *Biomacromolecules* **2007**, *8*, 1124–1130.
(37) Golan, R.; Pietrasanta, L. I.; Hsieh, W.; Hansma, H. G. *Biochemistry* **1999**, *38*, 14069–14076.
(38) Zelphati, O.; Nguyen, C.; Ferrari, M.; Felgner, J.; Tsai, Y.; Felgner, P. L. *Gene Ther.* **1998**, *5*, 1272–1282.
(39) Oupicky, D.; Konak, C.; Ulbrich, K.; Wolfert, M. A.; Seymour, L. W. *J. Controlled Release* **2000**, *65*, 149–171.
(40) Oupicky, D.; Bisht, H. S.; Manickam, D. S.; Zhou, Q.-h. *Expert Opin. Drug Deliv.* **2005**, *2*, 653–665.
(41) Vilfan, I. D.; Conwell, C. C.; Sarkar, T.; Hud, N. V. *Biochemistry* **2006**, *45*, 8174–8183.
(42) Siqian He, P. G. A.; Bloomfield, V. A. *Biopolymers* **2000**, *53*, 329–341.
(43) Dauty, E.; Remy, J. S.; Blessing, T.; Behr, J. P. *J. Am. Chem. Soc.* **2001**, *123*, 9227–9234.
(44) Gosule, L. C.; Schellman, J. A. *Nature* **1976**, *259*, 333–335.
(45) Bloomfield, V. A. *Curr. Opin. Struct. Biol.* **1996**, *6*, 334–341.
(46) Rolland, A.; Felgner, P. L. *Adv. Drug Delivery Rev.* **1998**, *30*, 1–3.
(47) Luo, D.; Saltzman, W. M. *Nat. Biotechnol.* **2000**, *18*, 33–37.
(48) Bloomfield, V. A. *Biopolymers* **1997**, *44*, 269–282.
(49) Todd, B. A.; Parsegian, V. A.; Shirahata, A.; Thomas, T. J.; Rau, D. C. *Biophys. J.* **2008**, *94*, 4775–4782.
(50) Wilson, R. W.; Bloomfield, V. A. *Biochemistry* **1979**, *18*, 2192–2196.
(51) Hansma, H. G. *Annu. Rev. Phys. Chem.* **2001**, *52*, 71–92.
(52) Yoshikawa, K.; Matsuzawa, Y. *J. Am. Chem. Soc.* **1996**, *118*, 929–930.
(53) Conwell, C. C.; Vilfan, I. D.; Hud, N. V. *Proc. Natl. Acad. Sci. U.S.A.* **2003**, *100*, 9296–9301.
(54) Noguchi, H.; Yoshikawa, K. *J. Chem. Phys.* **2000**, *113*, 854–862.
(55) Stevens, M. J. *Biophys. J.* **2001**, *80*, 130–139.
(56) Ou, Z. Y.; Muthukumar, M. *J. Chem. Phys.* **2005**, *123*, 074905.
(57) Vasilevskaya, V. V.; Khokhlov, A. R.; Kidoaki, S.; Yoshikawa, K. *Biopolymers* **1997**, *41*, 51–60.
(58) Akitaya, T.; Seno, A.; Nakai, T.; Hazemoto, N.; Murata, S.; Yoshikawa, K. *Biomacromolecules* **2007**, *8*, 273–278.
(59) Nguyen, T. T.; Shklovskii, B. I. *Phys. Rev. E* **2002**, *65*, 031409.
(60) Pouton, C. W.; Seymour, L. W. *Adv. Drug Delivery Rev.* **2001**, *46*, 187–203.
(61) Merdan, T.; Kopecek, J.; Kissel, T. *Adv. Drug Delivery Rev.* **2002**, *54*, 715–758.
(62) Jensen, K. S.; Hansen, R. E.; Winther, J. R. *Antioxidants and Redox Signaling*, 0.
(63) Whitesides, G. M.; Lilburn, J. E.; Szajewski, R. P. *J. Org. Chem.* **1977**, *42*, 332–338.
(64) Grosberg, A. Y.; Nguyen, T. T.; Shklovskii, B. I. *Rev. Mod. Phys.* **2002**, *74*, 329–345.

JP901835U